J Mater Sci (2006) 41:4389–4393
DOI 10.1007/s10853-006-0150-4

Atomic scale characterization of complex oxide interfaces

Maria Varela · Timothy J. Pennycook · Wei Tian · David Mandrus · Stephen J. Pennycook · Vanessa Peña · Zouhair Sefrioui · Jacobo Santamaria

Received: 20 December 2005 / Accepted: 1 March 2006 / Published online: 6 July 2006

Abstract Complex oxides exhibit the most disparate behaviors, from ferroelectricity to high T_c superconductivity, colossal magnetoresistance to insulating properties. For these reasons, oxide thin films are of interest for electronics and the emerging field of spintronics. But epitaxial complex oxide ultrathin films and heterostructures can be significantly affected or even dominated by the presence of interfaces and may exhibit intriguing new physical properties quite different from the bulk. A study of the relations between structure and chemistry at the atomic scale is needed to understand the macroscopic properties of such ''interface-controlled'' materials. For this purpose, the combination of aberration-corrected *Z*-contrast scanning transmission electron microscopy (STEM) and electron energy-loss spectroscopy (EELS) represents a very powerful tool. The availability of sub-Ångström probes allows a level of unprecedented detail when analyzing not only the interface structure with sensitivity to single atoms, but also the interface chemistry. In this work state of the art STEM-EELS will be applied to the study of different oxide interfaces in heterostructures with titanates, manganites and cuprates based on the perovskite structure.

M. Varela (✉) · T. J. Pennycook · W. Tian · D. Mandrus · S. J. Pennycook
Oak Ridge National Laboratory, BLDG 3025M, MS 6030, P.O. Box 2008, Oak Ridge, TN 37831, USA
e-mail: mvarela@ornl.gov

V. Peña · Z. Sefrioui · J. Santamaria
Universidad Complutense de Madrid, Avda. Complutense s/n, 28040 Madrid, Spain

Introduction

The physical properties of superlattices and heterostructures ultimately rely on the structure and chemistry of their interfaces, especially when the constituent layers are barely a few unit cells thick. In this case, the macroscopic properties usually differ strongly from the bulk, and in order to understand them a comprehensive structural and chemical analysis is needed. The success of aberration correction in electron microscopy has made sub-Ångström resolution [1] readily available with sensitivity to single atoms [2, 3], allowing us to take the analysis of structural, chemical and electronic properties of interfaces to the next level. This is particularly useful when analyzing oxide heterostructures. High-quality perovskite complex oxide thin films and superlattices are relatively easy to grow [4–7], as different perovskites are chemically compatible with each other and the lattice mismatch can be chosen to be small enough to promote good epitaxy. Also, they present many different kinds of physical behaviors ranging from high T_c superconductivity in cuprates to colossal magnetoresistance (CMR) in ferromagnetic manganese oxides. Therefore, superlattices based on these materials allow us to study the interaction between different, sometimes competing phenomena, as in ferromagnetic/superconducting superlattices where a high T_c superconductor is grown on top of a manganite with CMR properties. These kinds of heterostructures are interesting both from the fundamental and applied points of view, as it has recently been shown that they exhibit giant magnetoresistance [7]. Now more than ever, improving our understanding of such interactions relies on a careful atomic scale interface characterization. In this work we will address

the characterization of the structure and the chemistry of manganite based interfaces at the atomic level, including $SrTiO_3/La_{0.67}Ca_{0.3}MnO_3$ (STO/LCMO) and $YBa_2Cu_3O_{7-x}/La_{0.67}Ca_{0.3}MnO_3$ (YBCO/LCMO).

Methodical background and experimental setup

Scanning transmission electron microscopy (STEM) observations were carried out in a VG Microscopes HB603U operated at 300 kV and a VG Microscopes HB501UX operated at 100 kV, both equipped with Nion aberration correctors. The VG603 was not equipped with an EEL spectrometer at the time of this experiment, but the VG501 has a Gatan Enfina EELS. This microscope routinely achieves a spatial resolution of 0.11 nm and an energy resolution of about 0.35 eV [8]. Unless specified otherwise, all the data and images in this work were acquired in the VG501. The introduction of aberration correction allows both the imaging and spectroscopic identification of single atoms in bulk materials [2, 3, 8]. Also, it has enabled us to probe the structure, chemistry and electronic properties of solids with atomic resolution. For example, STEM-EELS is a powerful technique to study charge ordering phenomena in complex oxides. Figure 1a shows a *Z*-contrast image of a $Bi_{0.37}Ca_{0.63}MnO_3$ manganite along the cubic (1 0 0) zone axis. This material shows charge ordering (CO) at room temperature [9]. Because of strong intra-atomic Hund's rule interaction, the spins of the 3d electrons in the Mn atoms are aligned parallel to each other, forming the so called high-spin state, with three electrons in the t_{2g} orbitals and one extra electron in one of the e_g orbitals in Mn^{+3} atoms. CO in mixed valence manganites has been commonly interpreted as a spatial ordering of the e_g electrons, in other words an ordering in the Mn^{+3}/Mn^{+4} sublattices. EELS can successfully probe the 3d-band occupation in transition metal oxides, as the L edge of 3d metals is quite sensitive to the oxidation state. The ratio between the intensities of the L_3 and the L_2 lines, the L_{23} ratio, has been widely used to measure the Mn oxidation state in a series of compounds [10–12]. Figure 1b shows the L_{23} ratio measured when placing the electron beam on top of a Mn column and scanning it along the pseudocubic [1 0 0] direction while acquiring EEL spectra. The L_{23} ratio is observed to oscillate between the values of 2.1 (Mn^{+4}) and 2.7 (Mn^{+3}) with a periodicity of about 1.4 nm. This evidences the presence of stripes in the sample, which consist of an ordering of the occupation of the Mn 3d bands [13].

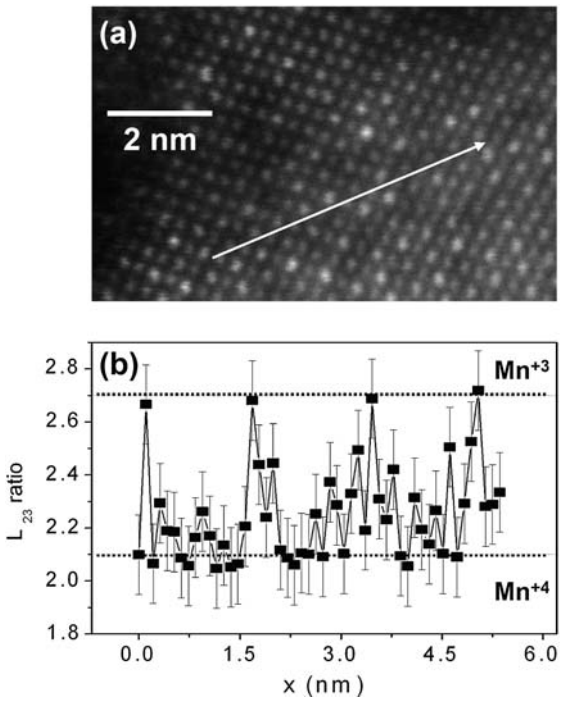

Fig. 1 Charge ordering in Mn oxides. (**a**) *Z*-contrast image of a $Bi_{0.37}Ca_{0.63}MnO_3$ manganite along the cubic (1 0 0) zone axis. (**b**) L_{23} ratio along an atomic row perpendicular to the direction (Data taken from ref. 8) marked with a white arrow in (**a**). The L_{23} ratio oscillates between the values corresponding to Mn^{+3} and Mn^{+4}, marked with horizontal dotted lines

Interface analysis with atomic resolution

Figure 2 shows a high-resolution image of a LCMO/STO interface. The image demonstrates a high-quality

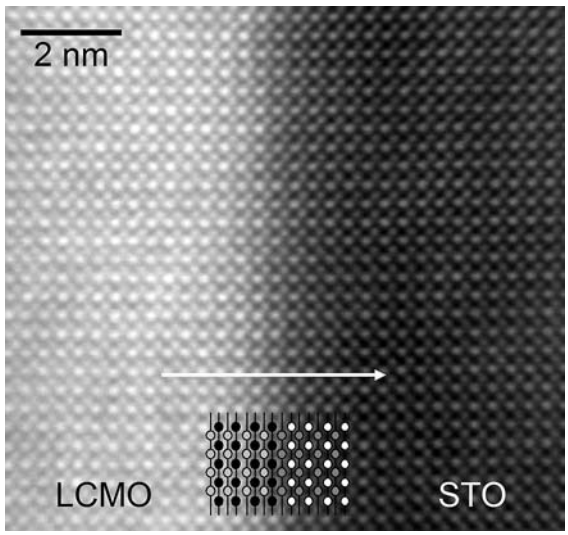

Fig. 2 *Z*-contrast image obtained in the VG501 of a $La_{0.67}Ca_{0.33}MnO_3/SrTiO_3$ interface along the cubic (1 0 0) zone axis. The interface atomic plane stacking sequence identified in the sketch is La/CaO (black) -MnO_2 (light grey)—La/CaO- TiO_2 (dark grey)—SrO (white)-TiO_2–SrO...

interface which is found to be coherent and free of defects. Figure 3a shows the intensity profile of the high-angle annular dark-field (HAADF) image across the interface. From these images, the interface does not look atomically sharp, as the background shows a very broad decay, about 1.5 nm wide (around 4 perovskite unit cells). This is more likely due to beam broadening through the specimen thickness due to dechanneling than to poor structural quality. But it is a major problem when it comes to trying to quantify the interface plane from the ADF images, as the tails of the probe make it difficult to identify which is the actual atomic plane stacking sequence at the interface. The intensity of a Z-contrast image is roughly proportional to Z^2, which should be enough to reveal the stacking, but the smearing of the image intensity across the interface together with the fact that the elements in discussion are very close in the periodic table make the identification problematic. Moreover, in a sample like this one, two different interface terminations are possible: ...La/CaO–MnO_2–SrO–TiO_2... versus ...MnO_2–La/CaO–TiO_2–SrO..., which may lead to very different physical properties in the sample [14, 15].

This question can be readily addressed by atomic resolution EELS. A high spatial resolution compositional analysis can be achieved by measuring the changes in the intensity of EELS signals corresponding to the different chemical elements of interest. The changes in the Ti $L_{2,3}$ edge at 456 eV, the La $M_{4,5}$ edge at 842 eV and the Mn $L_{2,3}$ edge at 644 eV (all of these edges energies are nominal values) can be monitored by placing the 0.11 nm electron beam at the interface and scanning across it. The intensities of the edges can be integrated and normalized to give a quantitative measurement of elemental concentration (the specimens used were thin, so the data have not been corrected for multiple scattering effects). For the LCMO/STO interface of Fig. 2, the chemical profiles of La (black squares), Mn (open circles) and Ti (open squares) are shown in Fig. 3b. When approaching the interface (marked with a vertical dotted line) from the LCMO side the Mn signal starts to decrease before the La does, resulting in the La concentration profile being offset by about 0.2 nm (roughly the width of one atomic plane). Within the STO, both signals go down to zero values. Meanwhile, the Ti concentration increases gradually. The observed delay of the La signal with respect to the Mn signal shows unambiguously that the interface stacking sequence is ...MnO_2–La/CaO–TiO_2–SrO...

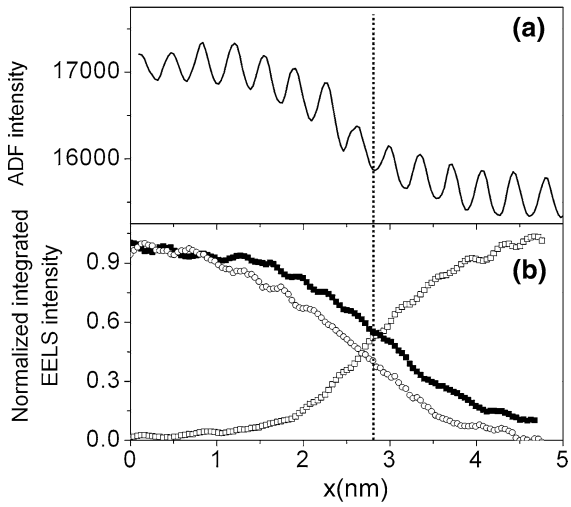

Fig. 3 (**a**) Linetrace showing the intensity of the HAADF image along a line parallel to the direction marked with a white arrow in Fig. 2. (**b**) Integrated, normalized EELS intensity when scanning the electron beam across the interface again along a line parallel to the direction marked with a white arrow in Fig. 2 for the Ti L edge (open squares), Mn L edge (open circles), and the La M edge (solid squares). The interface position has been marked with a vertical, dotted line

Also, all of the chemical signals in Fig. 3b show a well defined oscillation with a period equal to one lattice constant (roughly 0.38 nm). Each elemental concentration peaks on the atomic plane where that particular chemical species is located. For example, on the LCMO side of the interface, the concentrations of La and Mn oscillate out of phase. Therefore, this behavior is not an artifact resulting from the oscillation of the probe intensity when being respectively on and off column. The EELS intensity is proportional not only to the elemental concentration but also to the incoming beam intensity, which changes periodically (with an inverse dependence) with the HAADF signal. The observed modulation is a result of the spatial localization of the scattering processes for these high energy losses [16].

Ferromagnetic/superconducting oxide interfaces

In oxide heterostructures, the interface structure can ultimately determine the physical properties of ultrathin oxide layers. This is especially true for interfaces based on high T_c superconductors. These materials have very complex unit cells and even the smallest structural modifications (such as those induced by epitaxial strain) may have an effect on the doping and therefore on the superconducting properties [17–20]. This is particularly relevant when studying the properties of superconducting/ferromagnetic [$YBa_2Cu_3O_{7-x}$/$La_{0.67}Ca_{0.33}MnO_3$] (YBCO/LCMO) superlattices. In these samples, the interplay of superconductivity and

magnetism is going to be deeply affected by the interface properties.

Figure 4 shows a high-magnification HAADF image of a YBCO/LCMO interface. The structural quality is very high, the interface being coherent and free of defects. In the YBCO structure the CuO chain plane is the lightest in the unit cell, and is further away from the BaO plane than the CuO_2 layer. It therefore appears significantly darker in the image, while BaO planes show up with the brightest contrast. The CuO_2 planes can be observed sandwiched between them, together with the intermediate *Y* plane. All these atomic planes have been identified in Fig. 4. A close inspection of the interface structure suggests that the CuO chains are absent at the interface. EELS line scans confirm that this is the case indeed. Figure 5a shows the normalized integrated intensity under the Ba M edge at 781 eV (black circles), the Cu L edge at 931 eV (open triangles) and the Mn L edge (white squares) across the YBCO/LCMO interface. Again, the oscillation allows the location of the BaO, the CuO, and the MnO_2 atomic planes to be observed. Figure 5b shows the intensity of the HAADF image on the background (to scale).The background image is the same that the one shown in Figure 4 (from the VG603 microscope), and it was not acquired simultaneously with the EELS data (from the VG501). Therefore, the comparison with the HAADF image and intensity trace is included only for illustrative purposes. A straightforward cross check shows that the Ba signal as extracted from the EEL spectra peaks on the BaO planes in the image. Reciprocally, the Mn signal peaks on the MnO_2 planes. The Cu signal is a bit more noisy, due to the higher energy loss and poor signal-to-noise ratio of the measurements. However, it also seems to be modulated according to the atomic plane stacking. Furthermore, it clearly decays before the Ba signal does when approaching the interface (the offset is about 0.2 nm). Therefore, it is straightforward to unambiguously identify the interface stacking revealed by the *Z*-contrast images as ...CuO–BaO–Y–BaO–MnO_2–La/CaO–MnO_2.... This is a very relevant detail when it comes to understanding the physical properties of ultrathin YBCO layers in YBCO/LCMO superlattices. The CuO chains are essential to superconductivity as it is commonly believed that the holes responsible for superconductivity originate from the transfer of electrons from the CuO_2 planes into the CuO chains. Therefore, modifications in these chains (such as deoxygenation) have a deep impact on the properties. Heterostructures where very thin YBCO layers (1 or 2 unit cells thick) are sandwiched between LCMO layers are non superconducting [21], and this is because the CuO chains are missing. For YBCO/LCMO superlattices with YBCO layers nominally two unit cells thick there would be a complete, single layer of CuO chains shared between the two YBCO unit cells. However, it is unclear whether this isolated plane of CuO chains would be able to provide enough doping in the CuO_2 planes for superconductivity to happen.

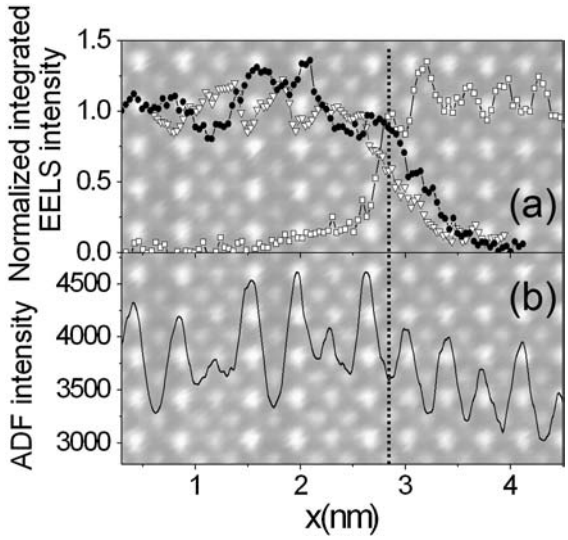

Fig. 5 Ba, Cu and Mn elemental profiles extracted from integrating the EELS intensity under the Ba M edge (solid circles), the Cu L edge (open triangles) and the Mn L edge (open squares) in a linescan across the YBCO/LCMO interface shown in Fig. 4. The image in the background is just intended to be a guide to the eye and it is to scale. EELS confirms the interface position, which has been marked with a vertical dotted line and it is clearly seen to be MnO_2

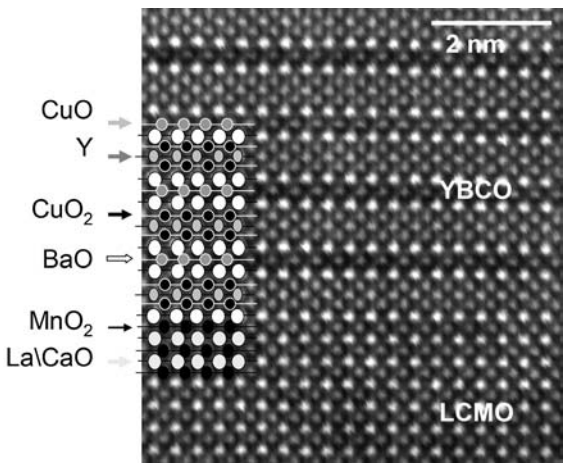

Fig. 4 *Z*-contrast image obtained in the VG603 of a YBCO/LCMO interface. The interface atomic plane stacking sequence is ...CuO–BaO–CuO_2–Y–CuO_2–BaO–La/CaO–MnO_2...

Conclusion

In summary, the combination of *Z*-contrast STEM and atomic-resolution EELS has shown to be a powerful tool for characterization of complex oxide interfaces. The chemical information provided by the EELS linescans has been observed to be modulated according to the chemical composition at the atomic scale, providing us with a unique tool to study complex oxide interfaces. In the LCMO/STO system the STO substrate has been shown to be TiO_2 terminated, and the manganite starts growing with a La/CaO plane. Meanwhile, the YBCO/LCMO interfaces do not have CuO interface chains, which will affect the superconducting properties of YBCO/LCMO superlattices when the YBCO thickness is 1 or 2 unit cells. We envise that this will most likely be the case when growing YBCO on other perovskite buffers.

Acknowledgements This research was sponsored by the Laboratory Directed Research and Development Program of ORNL, managed by UT-Batelle, LLC, for the U.S. Department of Energy under Contract No. DE-AC05-00OR22725. Financial support from the Spanish CICyT and the Fundacion Ramon Areces is acknowledged as well.

References

1. Nellist PD, Chisholm MF, Dellby N, Krivanek OL, Murfitt MF, Szilagi ZS, Lupini AR, Borisevich A, Sides WH, Pennycook SJ (2004) Science 305:1741
2. Varela M, Findlay SD, Lupini AR, Christen HM, Borisevich AY, Dellby N, Krivanek OL, Nellist PD, Oxley MP, Allen LJ, Pennycook SJ (2004) Phys Rev Lett 92:095502
3. Wang SW, Borisevich AY, Rashkeev SN, Glazoff MV, Sohlberg K, Pennycook SJ, Pantelides ST (2004) Nature Mater 3:143
4. Balestrino G, Lavanga S, Medaglia PG, Orgiani P, Tebano A (2002) Phys Rev B 66:094505
5. Triscone JM, Fischer O (1997) Rep Prog Phys 60:1673
6. Lee HN, Christen HM, Chisholm MF, Rouleau CM, Lowndes DH (2005) Nature 433:395
7. Peña V, Sefrioui Z, Arias D, Leon C, Santamaria J, Martinez JL, te Velthuis SGE, Hoffmann A (2005) Phys Rev Lett 94:057002
8. Varela M, Lupini AR, van K Benthem, Borisevich AY, Chisholm MF, Shibata N, Abe E, Pennycook SJ (2005) Ann Rev Mat Res 35:539
9. Woo H, Tyson TA, Croft M, Cheong S-W, Woick JC (2001) Phys Rev B 63:134412
10. Kurata H, Colliex C (1993) Phys Rev B 48:2102
11. Rask JH, Miner BA, Buseck PR (1987) Ultramicroscopy 21:321
12. Krivanek OL, Paterson JH (1990) Ultramicroscopy 32:313
13. Varela M et al. In preparation (2006)
14. Yamada H, Ogawa Y, Ishii Y, Sato H, Kawasaki M, Akoh H, Tokura Y (2004) Science 305:646
15. Ohtomo A, Muller DA, Grazul JL, Hwang HY (2002) Nature 419:378
16. Oxley MP et al. In preparation (2006)
17. Pickett W (1989) Rev Mod Phys 61:749
18. Klie RF, Buban JP, Varela M, Franceschetti A, Jooss C, Zhu Y, Browning ND, Pantelides ST, Pennycook SJ (2005) Nature 435:475
19. Varela M, Sefrioui Z, Arias D, Navacerrada MA, Lucia M, Lopez MA de la Torre, Leon C, Loos GD, Sanchez Quesada F, Santamaria J (1999) Phys Rev Lett 83:3936
20. Varela M, Arias D, Sefrioui Z, Leon C, Ballesteros C, Pennycook SJ, Santamaria J (2002) Phys Rev B 66:134517
21. Sefrioui Z, Varela M, Peña V, Arias D, Leon C, Santamaria J, Villegas JE, Martinez JL, Saldarriaga W, Prieto P (2002) Appl Phys Lett 81:4568